Single-angle compression members welded by one leg to a gusset plate. I. Experimental study

Murray C. Temple and Sherief S.S. Sakla

Abstract: Single-angle compression members are structural elements that are very difficult to analyze and design. These members are usually attached to other members by one leg only. Thus the load is applied eccentrically. To further complicate the problem the principal axes of the angle do not coincide with the axis of the frame of which the angle is a part. Although it is known that the end conditions affect the load-carrying capacity of these members, procedures have not been developed to account for this. The main objective of this research is to obtain a better understanding of the behaviour and load-carrying capacity of single-angle compression members welded by one leg to a gusset plate fixed to a rigid support. The effects of the gusset plate width, thickness, and the unconnected length were studied. It was determined that the finite element method can be used, with a reasonable degree of accuracy, to predict the behaviour and load-carrying capacity of these members. It was found that the thickness and width of the gusset plate significantly affect the load-carrying capacity, but the unconnected length has only a minor effect.

Key words: angles, buckling, building (codes), columns (structural), compressive resistance, design, gusset plates.

Résumé : Les membrures de compression à angle simple sont des éléments structuraux difficiles à analyser et à concevoir. Ces membrures sont généralement reliées à d'autres membrures par un seul membre. C'est pourquoi le chargement est appliqué excentriquement. De plus, pour compliquer le problème, l'axe principal de l'angle ne coïncide pas avec l'axe de la charpente dont il fait partie. Bien qu'il soit connu que les conditions de la base affectent la capacité portante de ces membrures, aucune procédure n'a été développée pour en tenir compte. Le objectif principal de cette étude est d'obtenir une meilleure compréhension du comportement et de la capacité portante des membrures de compression à angle simple soudées par une membrure à un gousset plat fixé au support rigide. L'effet de la largeur et de l'épaisseur du gousset plat ainsi que celui de la longueur non connectée ont été étudiés. Il a été déterminé que la méthode d'élément fini peut être utilisée, avec un degré de précision raisonnable, afin de prédire le comportement et la capacité portante de ces membrures. Il a été découvert que l'épaisseur et la largeur du gousset influent sensiblement sur la capacité portante, mais que la longueur non connectée a seulement un effet mineur.

Mots clés : angles, gauchissement, édifices (codes), colonnes (structurale), résistance en compression, conception, gousset plat.

[Traduit par la Rédaction]

Introduction

Single angles are one of the most basic of the hot rolled steel shapes. They are being used extensively in many structural applications. Steel angles can be very conveniently joined at their ends to gusset plates, webs of tees, or other structural elements. These joints are usually either shop welded or field bolted or welded. Welded gusset plate connections are widely used in braced steel frames in commercial and industrial buildings, as welds offer the best method of making rigid connections resulting in a reduced member size and weight. A typical gusset plate connection in a rigid frame is shown in Fig. 1*a* and a detail of the connection is shown in Fig. 1*b*.

Received April 15, 1997.
Revised manuscript accepted October 27, 1997.

M.C. Temple and S.S.S. Sakla. Department of Civil and Environmental Engineering, University of Windsor, Windsor, ON N9B 3P4, Canada.

Written discussion of this article is welcomed and will be received by the Editor until October 31, 1998 (address inside front cover).

In spite of the apparent simplicity of single-angle compression members, they are amongst the most complex structural members to analyze and design, especially when attached by one leg as the load is applied eccentrically to the angle. In addition, the principal axes of the angle cross section do not coincide with the axis of the frame to which the angle is connected. Since angles are connected to gusset plates or other structural members, the problem is further complicated by the fixity that exists at the ends of the angle. This fixity, in most practical cases, is hard to account for, since the magnitude of the end restraint is not known. The magnitude of this restraining end moment for a given angle size is a function of the gusset plate thickness, width, and length.

This research examines the load-carrying capacity and behaviour of a single-angle compression member welded by one leg to a gusset plate fixed to a rigid support. The rigid support is of the type that would be developed when a gusset plate is welded to the junction of a beam and column as shown in Fig. 1*a*. This research is applicable to single-angle compression members which are used in low rise buildings or in the upper storeys of higher buildings where the wind shear is low. The research is not applicable to angles in

Fig. 1. Typical gusset plate connection: (*a*) gusset plate connection; (*b*) detail of connection showing the geometric and principal axes.

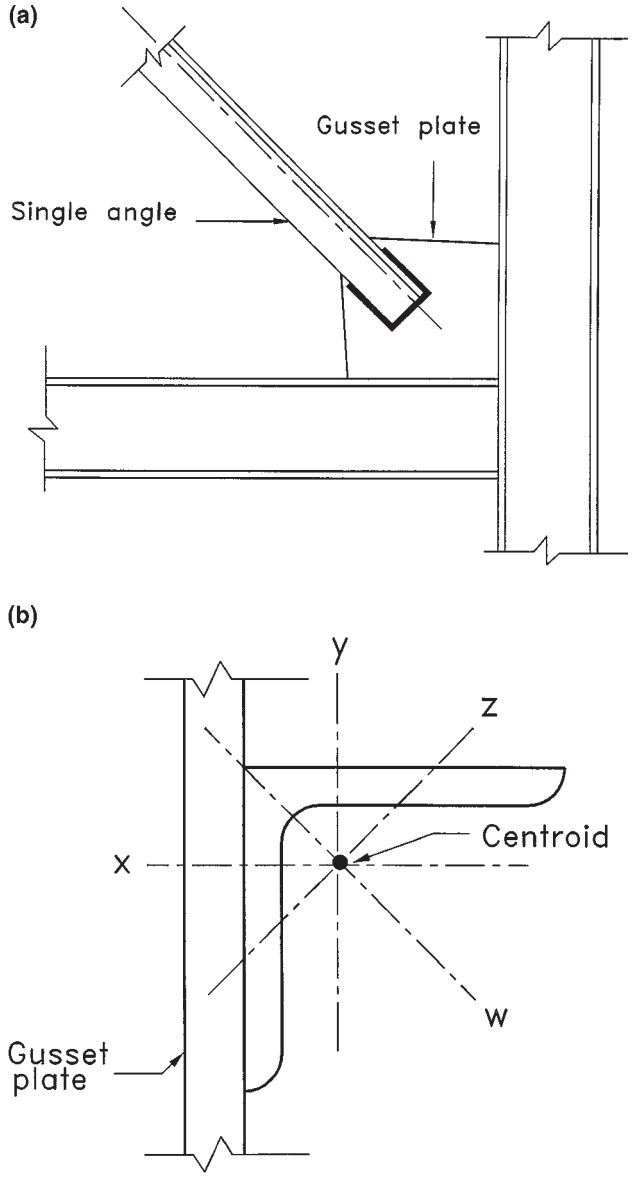

trusses, to double-angle compression members, or to the case where several angles are attached to a gusset plate. The research is applicable only to hot rolled steel angles.

Design practices

A study by Temple and Sakla (1996) showed that design practices vary greatly in the way they deal with the design of single-angle compression members. In that research, the results of an experimental study carried out by Trahair et al. (1969) were utilized to evaluate current design practices and design procedures proposed in previous research. It was concluded that compressive resistances vary greatly depending on the standard or specification used to predict them. In most cases, the compressive resistances differ significantly from the experimental results. The CISC *Handbook of Steel Construction* (CISC 1995) provides no explicit guidance as to a preferred design procedure for these compression members. Past practice in Canada seems to be to design such members as concentrically loaded pin-ended columns that buckle about the minor principal axis of the cross section with an effective length factor that is usually taken as 1.0. The AISC *Manual of Steel Construction, Load and Resistance Factor Design* (AISC 1994) more explicitly recommends that such members be designed for biaxial bending. The load is assumed to act at the centre of the gusset plate, and the moments about the principal axes are calculated accordingly.

Although the AISC load and resistance factor design beam-column approach seems to reflect the expected behaviour of single angles as beam-columns, it underestimates the load-carrying capacity and results in a conservative solution. This seems to be due, in part, to neglecting the end fixity. This end fixity could be of the type shown in Fig. 1*a* where the angle is welded to a gusset plate.

It can be seen that the simple-column approach is not a rational approach. The assumptions used in this approach do not correspond to the behaviour of single angles observed in experimental testing. With the great variation between different design practices in the prediction of the compressive resistances of single-angle compression members, it is difficult to determine the most appropriate design procedure.

To further complicate the design of single angles attached by one leg to a gusset plate, the load-carrying capacity of these single-angle compression members varies significantly when the gusset plate dimensions are changed. The ultimate load-carrying capacity increases considerably if, for example, the gusset plate thickness or width is increased. Changing the gusset plate dimensions changes the restraining moments provided by the gusset plates to the ends of the angle. This changes the apparent location of the load in such a way that it is closer to the centroid. This is why the simple-column approach yields results that are in much better agreement, in most cases, than those predicted using the AISC beam-column approach.

As can be noted from the discussion above, none of the current design procedures accurately predicts the ultimate load-carrying capacity of single-angle compression members welded by one leg to a gusset plate. There is no published research that relates the gusset plate dimensions to the ultimate load-carrying capacity of single-angle compression members. Such a study is crucial to define the most influential design parameters that affect the ultimate load-carrying capacity.

Research objectives

The main objective of this study is to obtain a better understanding of the behaviour of single-angle compression members welded by one leg to a gusset plate. The effects of changing the unconnected length, width, and thickness of the gusset plate were studied. The unconnected length of the gusset plate is defined as the distance from the end of the angle to the section at which a plastic hinge forms. In the test specimens the end of the gusset plate is considered to be the start of the fillet between the flange and web of the tee section. The study investigated the use of the finite element method for predicting the behaviour and ultimate load-

carrying capacity of this type of structural member. The experimental specimens were modelled and the finite element results were compared with those obtained experimentally.

Using the finite element analysis allows the study of the effect of some parameters, such as initial out-of-straightness and residual stresses, that cannot be studied economically by experimental testing. A finite element analysis is also used to generate a wide range of numerical models in order to obtain enough data for use in the development of design curves or equations. In a companion paper the results of the parametric study and a proposed design procedure are presented (Temple and Sakla 1998).

Literature review

Leigh and Galambos (1972) carried out tests on compression webs of long span steel joists. It was observed that the dominant deflection of the angle compression webs occurred in a direction perpendicular to the connected leg. They proposed two empirical design procedures. The first design procedure was based on a simplified ultimate strength interaction equation. The authors suggested that the problem should be treated as a uniaxial bending beam-column problem and that the slenderness ratio should be based on r_y, where r_y is the radius of gyration about the y axis, that is, the geometric axis parallel to the connected leg (see Fig. 1*b*). The AISC beam-column interaction equation is then used to evaluate the axial compressive load-carrying capacity as follows:

$$[1] \qquad \frac{P}{P_o} + \frac{C_m M_1}{M_y\left[1 - \frac{P}{P_E}\right]} = 1$$

where P is the axial compressive load; P_o is the axial load-carrying capacity in the absence of bending; M_y is the moment about the y axis required to produce compressive yielding in the extreme fibre when the axial load is zero; M_1 is the largest bending moment acting at the end of the member taking into account the end restraint caused by the truss chords; $C_m = 0.6 - 0.4(M_2/M_1)$, where M_1 and M_2 are the member end moments and M_1 is numerically greater than M_2; and P_E is the Euler load about the y axis.

It was found that this equation gave satisfactory, if somewhat conservative, predictions of the actual load-carrying capacity, provided that the end eccentricities were reduced to account for the end restraints. The problem is that it is difficult to account for this reduction in end eccentricity, since the end restraint is not easy to evaluate. This procedure has not been widely adopted by practising engineers, since it involves the use of the beam-column equation, which is a fairly lengthy procedure for what appears to be a simple structural element.

The above equation has also been recommended for the design of single-angle web members of trusses whose ends are connected to the chords by welding or by a multiple bolted connection (Woolcock and Kitipornchai 1980, 1986). Once again, care is required when deciding upon appropriate end moments if these end moments are to reflect, as accurately as possible, the effects of load eccentricity.

The other empirical design equation proposed by Leigh and Galambos (1972) is a simplified form of the uniaxial bending beam-column approach. This procedure equates the applied compressive stress to the Column Research Council stress equation in effect at that time (Johnston 1966). The applied compressive stress is the sum of the stress due to the axial load and the flexural stress caused by the eccentricity of the applied load. The flexural stress, as mentioned before, is based on bending about the geometric axis parallel to the attached leg, the y axis. This equation is written as

$$[2a] \qquad F_a = \frac{P}{A} + \frac{C_m M_1 y}{I_y}$$

and

$$[2b] \qquad F_{CRC} = F_y\left[1 - \frac{F_y(KL/r_y)^2}{4\pi^2 E}\right]$$

where F_a is the applied compressive stress due to the axial load and bending; A is the cross-sectional area of the angle; y is the distance from the centroid of the angle to its compressive edge; I_y is the moment of inertia about the y axis; F_{CRC} is the Column Research Council basic column strength formula; F_y is the yield stress; K is the effective length factor; L is the length of the angle; and E is Young's modulus of elasticity.

Experimental procedure

General

An experimental program was carried out to obtain data that were used to verify the theoretical results obtained from the finite element model. The experimental program was designed to study the effect of gusset plate dimensions on the load-carrying capacity and behaviour of single-angle compression members attached to a gusset plate by one leg with welds. These variables were not included in the Trahair et al. (1969) experimental study. The experimental program consisted of 33 ultimate strength tests of single-angle members connected to tee sections. The webs of the tee sections were used to simulate gusset plates. A typical test specimen is shown in Fig. 2. The angles were designed according to Standard CAN/CSA-S16.1-M89, "Limit states design of steel structures" (CSA 1989). In order to reduce the number of variables in this research, the same size angle was used for all tests. Three different lengths of angles, 2100, 1550, and 990 mm, were used. This resulted in slenderness ratios, L/r_z, of 170, 125, and 80, where r_z is the radius of gyration about the z axis, the minor principal axis. A typical specimen, as shown in Fig. 2, consisted of a single-angle member welded to a tee section at each end. The compression members were made from 64 × 64 × 7.9 mm (2½ × 2½ × 5/16 in.) angles and tee sections were cut from either a W530 × 82 (a W21 × 55 in imperial units) or a W530 × 123 (W21 × 83) depending on the required gusset plate thickness. Table 1 gives a full description of the dimensions of all the specimens tested in this study. The centroidal x axis of the angles coincided with the centre of the tee sections. Twelve slender specimens were tested. Twenty-one specimens of intermediate lengths

Fig. 2. Typical test specimen.

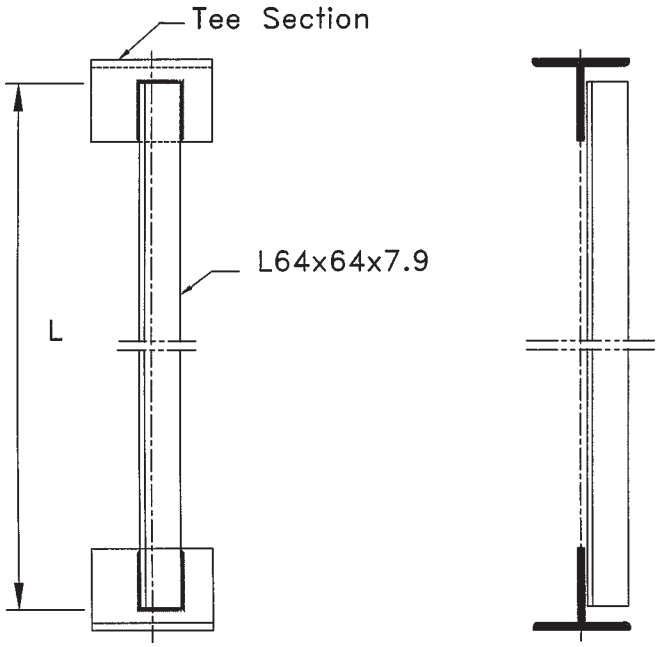

were tested with nine of the specimens being longer than the other twelve.

For the slender specimens and for the shorter intermediate length specimens, three different variables were investigated: (*i*) unconnected length of the gusset plate, L_g; (*ii*) the gusset plate width, B_g; and (*iii*) the gusset plate thickness, t_g. For the longer intermediate length specimens, only the effects of the gusset plate width and thickness were investigated.

Preparation of test specimens

The angle members were cut from 6.1 m (20 ft) lengths of angles. The tee sections were prepared by splitting the W sections longitudinally into two equal sections. These tee sections were then cut to the proper length and were machined at both ends to ensure that they were the same length and that the ends were perpendicular to the longitudinal axis of the tee section. The final length after machining was either 150 or 225 mm depending on the specimen type. Four guide holes were drilled in the flanges of the tee sections to accommodate countersunk bolts and were used for the alignment of the specimens.

The tee sections, in all specimens, were attached to the upper and lower platens of the testing frame and held firmly in place by the countersunk bolts. The angle was then welded to the tee sections. This procedure follows, as closely as possible, the procedure used to fabricate trusses or to erect bracing members in frames.

Test procedure

All the tests were carried out in the Civil Engineering Structures Laboratory at the University of Windsor. The Gilmore load fatigue frame was used for the testing, as it could be adjusted to accommodate the different lengths of the test specimens. The test setup is shown in Fig. 3.

Fixed end conditions were created at the ends of the specimen. This was achieved by bolting the tee sections directly to the platens of the Gilmore load fatigue frame. The end fixtures were designed to eliminate lateral displacements and rotations about each of the three global axes at the ends of the specimen. This end condition corresponds to the case where an angle is used as a bracing member and is welded to a gusset plate which in turn is welded to the intersection of a column and a beam.

The four holes in the upper and lower plates were used to firmly fix the specimen to the end plates. This achieved three purposes: (*i*) they were used to guide the specimen into the upper and lower plates, which were fixed to the upper and lower platens of the Gilmore load fatigue frame to ensure that the centroid of the specimen coincided with the load applied to the specimen by the hydraulic jack; (*ii*) tightening these bolts ensured the elimination of any gap that might exist between the specimen and the loading plates; and (*iii*) this procedure ensured fixed end conditions at the ends of the specimen, as there were four points which were prevented from any lateral displacement or rotation during the application of the load to the specimen. In addition to these main purposes, the countersunk bolts also prevented the ends of the specimens from slipping or kicking out during testing.

At the base, the load was applied to the specimens through a computer-controlled hydraulic jack with a capacity of 448 kN (100 kips). A Strainsert flat load cell with a 448 kN (100 kips) capacity was used to determine the load and was attached to the top platen of the Gilmore load fatigue frame. The load cell was connected to a data acquisition system that converted the voltage readings to a load at any instant during the application of the load. A steel plate similar to the one attached to the loading jack was fabricated and attached to the underside of the load cell with guiding holes to provide a connection to the top of the test specimen.

Three dial gauges at mid-height of the specimen, as illustrated in Fig. 4, were used to measure displacements and rotations. Two other dial gauges were placed on the web of one of the tee sections at the end of the angle. The purpose of these dial gauges was to measure the lateral deflection and the rotation of each angle to determine the effect of each gusset plate variable on both the magnitude of the deflection and the position of the failure axis.

In order to get more confidence in the results obtained from the finite element model, one slender specimen, L-A-3, and one shorter intermediate length specimen, S-A-3, were strain gauged as shown in Fig. 5 to study the behaviour of the ends of the gusset plate and the angle cross section at mid-height. The notation used to designate each specimen is defined in Table 1.

The out-of-straightness of each leg of each angle was measured prior to the application of the load using two steel blocks, a thin wire, and a digital calliper. The specimens were coated with a thin layer of whitewash before testing in order to detect the yield pattern as the load was increased. The specimen was now ready to be placed in the test frame. A small load of approximately 8 kN was applied to the specimen at the beginning to ensure that the top and lower plates were in complete contact with the ends of the specimen. The countersunk bolts were tightened. The preload was then released to almost zero. Dial gauges were positioned and set to zero before loading started.

Table 1. Dimensions of test specimens.

Specimen* (1)	Gusset plate: Width B_g (mm) (2)	Gusset plate: Thickness t_g (mm) (3)	Gusset plate: Unconnected length L_g (mm) (4)	Angle length L (mm) (5)	Weld length L_w (mm) (6)
L-A	150	10.2	20	2100	35
L-B	150	10.2	40	2100	35
L-F	150	12.7	20	2100	35
L-J	225	10.2	20	2100	35
M-A	150	10.2	20	1550	60
M-F	150	12.7	20	1550	60
M-J	225	10.2	20	1550	60
S-A	150	10.2	20	990	78
S-B	150	10.2	40	990	78
S-F	150	12.7	20	990	78
S-J	225	10.2	20	990	78

*The first letter refers to the length of the angle member. L, M, and S refer to specimens with angle lengths of 2100, 1550, and 990 mm, respectively. The second letter refers to specific gusset plate dimensions, for example, A refers to a gusset plate with a 150 mm width, a 10.2 mm thickness, and a 20 mm unconnected length. When a number follows the notation the number indicates the number of the specimen of the same type.

Fig. 3. Test setup.

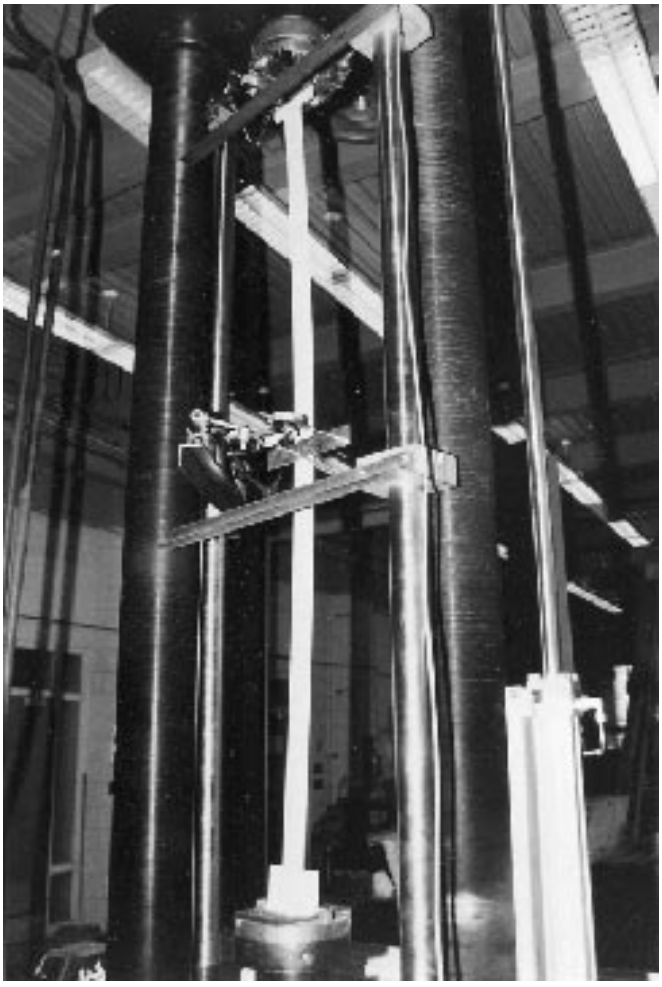

Fig. 4. Location of dial gauges.

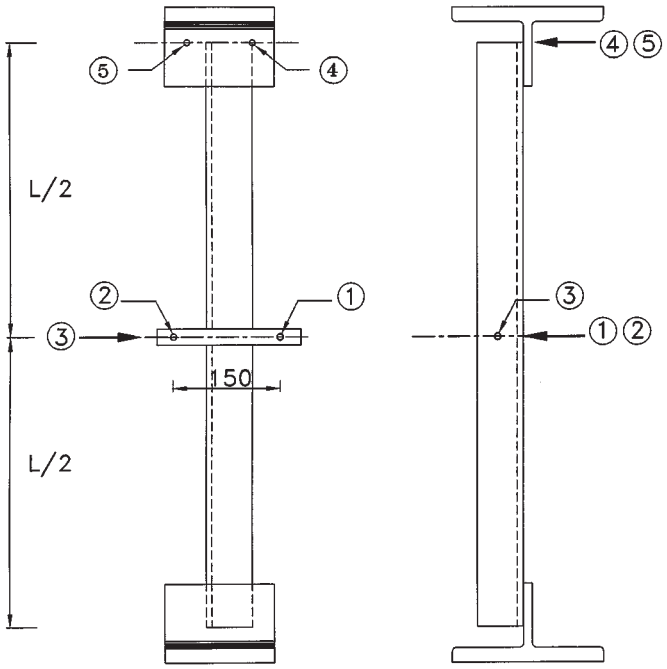

The load on the specimens was applied in increments of 5 kN for slender specimens and 10 kN for intermediate length specimens. This load increment was reduced to 2 kN for slender specimens and 3 kN for intermediate length specimens after reaching 70% of the expected failure load.

In all cases, the system was allowed to reach equilibrium, the point at which the lateral displacements stopped increasing, within acceptable limits, at a given load, prior to reading the dial gauges. A typical test took an average of 2 hours to complete both the setup and testing.

Finite element analysis

A commercial finite element package, ABAQUS (Hibbitt, Karlson and Sorenson, Inc. 1994), was used to perform a nonlinear static analysis. Both material and geometric nonlinearities were considered in the analysis of the speci-

Fig. 5. Location of strain gauges. (All dimensions are in millimetres.)

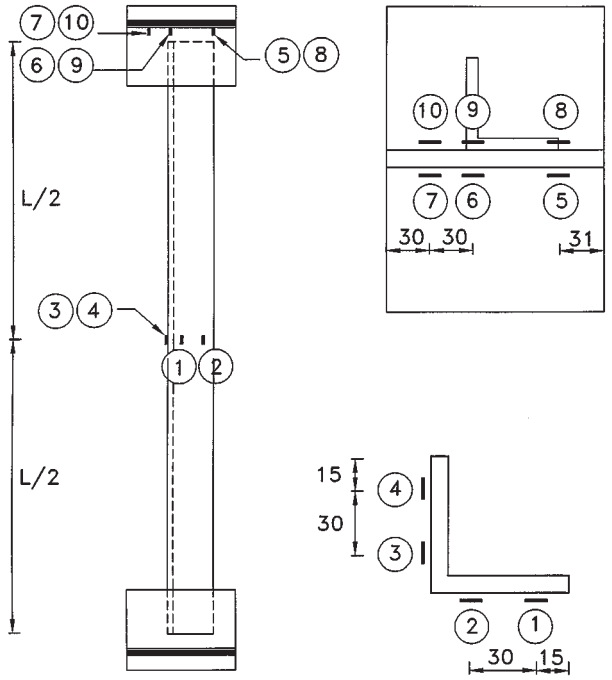

mens. Residual stresses due to the rolling of the angles were considered to determine their effects, but local residual stresses due to the welding of the specimen were excluded from the analysis because of the difficulty in determining such stresses. It is realized that residual stresses due to the rolling process and (or) due to welding may be important in the zone where a plastic hinge forms in the gusset plate. It will be pointed out, however, that the good agreement between the finite element and the experimental results indicates that these residual stresses do not have a significant effect on the results.

A convergence study was carried out in order to choose an appropriate finite element mesh. In order to save time it was decided to model only half the specimen with appropriate boundary conditions to reflect symmetry.

As the load transfers to the angle member, first through the gusset plate, through the welds to the connected leg, and then to the entire cross section, it was crucial to choose a mesh with a finer grid at the gusset plates and at the ends of the angle in order to model, more accurately, the distribution of stresses that takes place in this zone. The global axes were taken such that the cross section of the angles was in the *x*-*y* plane. A typical finite element mesh is shown in Fig. 6.

The load was applied at the ends of the gusset plate in the form of concentrated nodal loads. In order to allow for a uniform stress distribution at the end of the gusset plate, which is line 2 in the model, the loads were applied through a layer of linear elastic elements which are bounded between lines 1 and 2 in Fig. 6.

For the angles, it was decided to use eight four-node plate elements per leg. Discretizing the leg into eight strips of elements along the length enabled the modelling of residual stresses (although these were neglected later). From the pilot runs, it was found that an element aspect ratio less than 3 had to be maintained for all the elements in order to have consistent results.Thus the procedure followed to choose the relevant mesh for this problem was as follows: (*i*) a convergence test was carried out for the regular mesh and the appropriate number of elements was selected; and (*ii*) then more refined meshes were created at the end elements of the angle and the gusset plate to make it possible to model the stress distribution and the exact lengths of the welds.

The coordinates of the nodes of the model were defined taking into consideration the initial out-of-straightness of the angle. When modelling the experimental test specimens, the actual measured initial out-of-straightnesses were used.

The simple linear elastic, perfectly plastic stress–strain relationship was used for modelling the mechanical properties of the steel, assuming that the yield surface acts as a failure surface with no strain-hardening parameters. The Von Mises yield criterion for isotropic metals is used to model the plastic behaviour of the steel. Both Young's modulus of elasticity and the yield stress obtained from the tension tests were used in the analysis of the experimental test specimens.

Boundary conditions were imposed on two different groups of nodes in the model. The first group included all the nodes on lines 1 and 2 at the end of the gusset plate (see Fig. 6). At these nodes the displacements in both the *x* and *y* directions were prevented but the vertical displacements in the *z* direction were allowed. The three rotations about the global axes were prevented to represent the fixed end conditions at the end of the test specimen. The second group of nodes with imposed boundary conditions were the nodes at mid-height of the angle, on the plane of symmetry. For these nodes the displacements in the *z* direction, as well as the rotations about the *x* and *y* axes, were prevented.

A literature survey was conducted to determine if there is any published research in which a finite element model was used to model a weld subjected to both shear forces and bending moments perpendicular to the plane of weld. This survey revealed that the weld is either neglected and the material is considered to be continuous, or the weld material is assumed to be very rigid (Girard et al. 1995; Lipson and Haque 1978). The latter assumption was used in this research. The modelling of the welds was performed using the multi-point constraints (MPC) feature in ABAQUS. This option allows the imposing of constraints between specified degrees-of-freedom in the model. A BEAM MPC was used between all the welded nodes on the gusset plate and the corresponding nodes on the angle. This option connected two adjacent weld nodes with a very stiff beam.

Residual stresses develop in hot rolled sections as a consequence of the differential cooling process. It has been shown previously that the residual stresses affect the ultimate load-carrying capacity of angles connected by one leg by about 5% or less (Elgaaly et al. 1992; Usami and Galambos 1971). In spite of this, it was decided to check the effect the initiation of yielding of some parts of the member before others has on the load-carrying capacity of the specimens being studied. The residual stresses were modelled as an initial stress in the angle plate elements in the *z* direction. As part of the analysis procedure, ABAQUS performed an equilibrium check on the model under the imposed initial residual stresses. The ECCS (1985) recommendations regard-

Fig. 6. Finite element mesh. (All dimensions are in millimetres.)

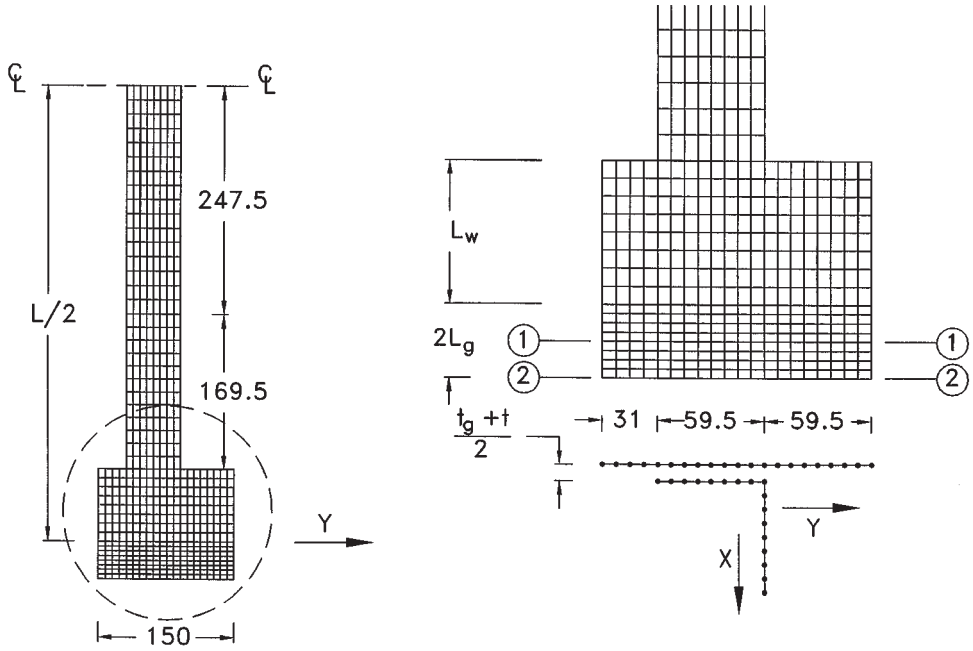

ing residual stresses were adopted in this study and are illustrated in Fig. 7.

Fig. 7. ECCS residual stresses.

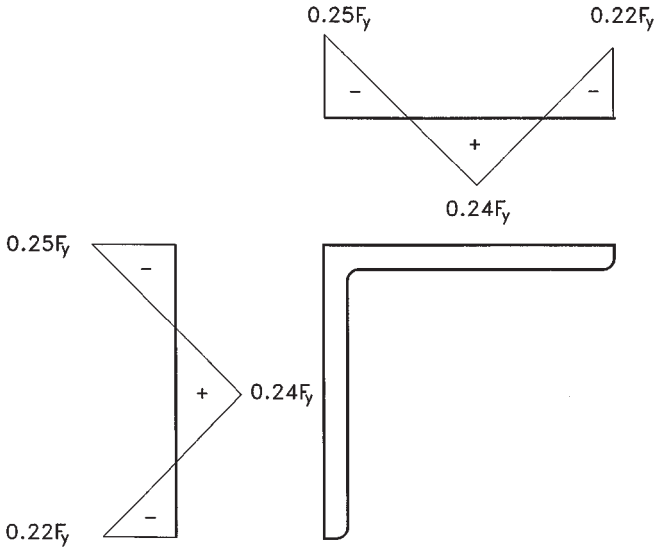

Results

Geometric and mechanical properties

Steel angles of nominal size 64 × 64 × 7.9 mm (2½ × 2½ × 5/16 in.) were used to build the specimens. In ABAQUS the geometric properties of the angles were calculated based on the idealized rectangular cross-sectional elements in which the toe and the fillet radii were omitted. The actual dimensions of the angles varied from the nominal dimensions by –0.2% to 1.1% for the angle leg widths and by –2.5% to 2.2% for the angle thicknesses. For convenience, the nominal dimensions were used for the finite element calculations.

Fifteen tension tests were carried out to determine the mechanical properties of the angles used in this experimental investigation. A tension specimen was prepared from each of the 15 pieces of angle, 6.1 m (20 ft) long, used in the experimental program. The tension specimens were prepared in accordance with the requirements of CAN/CSA-G40.20-M92, "General requirements for rolled or welded structural quality steel" (CSA 1992). Young's modulus of elasticity was determined by using strain gauges, one on each side of three tension test specimens.

For the angles, the average Young's modulus of elasticity was found to be 207 000 MPa and was used in all the theoretical computations. The yield stress varied from 344.8 to 417.1 MPa. Due to the significant difference in these values, the actual yield stress for each individual angle was used in the finite element analysis.

Three tension test specimens were taken from each of the W530 × 82 (W21 × 55) and W530 × 123 (W21 × 83) used in the specimens to represent the end gusset plates. For the W530 × 82 the yield stress varied from 404.7 to 423.3 MPa, and for the W530 × 123 the yield stress varied from 381.6 to 391.4 MPa. The average yield stresses were 413.4 and 386.6 MPa and were used in the finite element analysis, since they were within 2.3% of the actual values. The average Young's modulus of elasticity was found to be 203 400 and 204 100 MPa, respectively.

Initial out-of-straightness

The initial out-of-straightness of each leg of each angle was measured. The initial out-of-straightness ranged from *L*/930 to *L*/9130 for the slender specimens, from *L*/1000 to *L*/4430 for the longer intermediate length specimens, and from *L*/1830 to *L*/4125 for the shorter intermediate length specimens. For the angles used in the test specimens in the experimental program, the out-of-straightness, in general, decreased as the length of the angle decreased.

Table 2. Experimental and finite element results for slender specimens.

Specimen	P_{expt} (kN)	Average P_{expt} (kN)	$\frac{\text{Avg. } P_{expt}}{\text{Avg. } P_{expt\ A}}$ *	P_{theo} (kN)	$\frac{P_{theo} - P_{expt}}{P_{expt}}$ (%)	P_{theo} † (kN)	$\frac{P_{theo\ L/1000}}{P_{theo\ L/1000A}}$ ‡
(1)	(2)	(3)	(4)	(5)	(6)	(7)	(8)
L-A-1	89.3	89.6	1.000	95.7	7.2	82.9	1.000
L-A-2	90.1			93.8	4.1	82.9	
L-A-3	89.5			96.6	7.9	82.9	
L-B-1	85.8	86.5	0.965	92.4	7.7	80.6	0.972
L-B-2	86.5			93.3	7.9	80.6	
L-B-3	87.3			90.6	3.8	80.6	
L-F-1	103.7	103.3	1.153	109.4	5.5	93.4	1.127
L-F-2	101.2			109.7	8.4	93.4	
L-F-3	105.1			108.3	3.0	93.4	
L-J-1	99.3	101.2	1.129	104.1	4.8	89.0	1.074
L-J-2	100.2			104.1	3.9	89.0	
L-J-3	104.1			106.8	2.6	89.0	

*Ratio of average experimental failure load to average experimental failure load for slender specimens with a gusset plate width of 150 mm, thickness of 10.2 mm, and an unconnected length of 20 mm (a type A gusset plate).

† Finite element failure load of a specimen with an out-of-straightness of $L/1000$.

‡ Ratio of finite element failure load of a specimen with an out-of-straightness of $L/1000$ to finite element failure load for a slender specimen with the same out-of-straightness and a gusset plate width of 150 mm, thickness of 10.2 mm, and an unconnected length of 20 mm (a type A gusset plate). F_y = 300 MPa.

Table 3. Experimental and finite element results for longer intermediate length specimens.

Specimen	P_{expt} (kN)	Average P_{expt} (kN)	$\frac{\text{Avg. } P_{expt}}{\text{Avg. } P_{expt\ A}}$ *	P_{theo} (kN)	$\frac{P_{theo} - P_{expt}}{P_{expt}}$ (%)	P_{theo} † (kN)	$\frac{P_{theo\ L/1000}}{P_{theo\ L/1000A}}$ ‡
(1)	(2)	(3)	(4)	(5)	(6)	(7)	(8)
M-A-1	131.4	130.7	1.000	136.5	3.9	110.6	1.000
M-A-2	128.7			136.5	6.1	110.6	
M-A-3	132.1			135.0	2.2	110.6	
M-F-1	146.1	141.8	1.085	146.4	0.2	121.5	1.099
M-F-2	135.0			140.1	3.8	121.5	
M-F-3	144.3			145.5	0.8	121.5	
M-J-1	141.0	137.9	1.055	139.4	–1.1	115.5	1.045
M-J-2	137.2			138.6	1.0	115.5	
M-J-3	135.4			138.6	2.4	115.5	

* Ratio of average experimental failure load to average experimental failure load for longer intermediate length specimens with a gusset plate width of 150 mm, thickness of 10.2 mm, and an unconnected length of 20 mm (a type A gusset plate).

† Finite element failure load of a specimen with an out-of-straightness of $L/1000$.

‡ Ratio of finite element failure load of a specimen with an out-of-straightness of $L/1000$ to finite element failure load for a longer intermediate length specimen with the same out-of-straightness and a gusset plate width of 150 mm, thickness of 10.2 mm, and an unconnected length of 20 mm (a type A gusset plate). F_y = 300 MPa.

Experimental and theoretical results

Tables 2–4 list the ultimate load-carrying capacities obtained from the experimental program and from the finite element analysis. Although the theoretical failure loads obtained from the finite element method are, in general, higher than the experimental failure loads, the agreement is quite good. The difference ranged from +2.6% to +8.4% for the slender specimens, from –1.1% to +6.1% for the longer intermediate length specimens, and from +3.1% to +8.7% for the shorter intermediate length specimens. It can be concluded that the finite element analysis can be used to predict, with a reasonable degree of accuracy, the ultimate load-carrying capacity of single-angle compression members welded by one leg to a gusset plate.

Table 5 makes a comparison of the experimental failure loads and the compressive resistances predicted by using the two generally accepted design approaches. The design equations for the simple-column approach are given in clause 13.3.1 of S16.1-M89 (CSA 1989) and the equations for the beam-column approach in chapter H of the AISC load and resistance factor design specification (AISC 1994). The two design approaches have been explained in detail in a paper

Table 4. Experimental and finite element results for shorter intermediate length specimens.

Specimen	P_{expt} (kN)	Average P_{expt} (kN)	$\frac{\text{Avg. } P_{expt}}{\text{Avg. } P_{expt\ A}}$ *	P_{theo} (kN)	$\frac{P_{theo} - P_{expt}}{P_{expt}}$ (%)	P_{theo} † (kN)	$\frac{P_{theo\ L/1000}}{P_{theo\ L/1000\,A}}$ ‡
(1)	(2)	(3)	(4)	(5)	(6)	(7)	(8)
S-A-1	163.3	163.5	1.000	174.4	6.4	141.2	1.000
S-A-2	161.9			176.4	8.2	141.2	
S-A-3	165.4			181.2	8.7	141.2	
S-B-1	156.0	157.2	0.961	170.4	8.5	138.8	0.983
S-B-2	160.7			172.4	6.8	138.8	
S-B-3	155.0			165.0	6.1	138.8	
S-F-1	172.9	174.4	1.066	184.8	6.4	151.6	1.074
S-F-2	179.2			185.0	3.1	151.6	
S-F-3	171.1			185.8	7.9	151.6	
S-J-1	180.6	179.8	1.099	193.2	6.5	152.4	1.079
S-J-2	176.7			191.6	7.8	152.4	
S-J-3	182.1			196.4	7.3	152.4	

* Ratio of average experimental failure load to average experimental failure load for shorter intermediate length specimens with a gusset plate width of 150 mm, thickness of 10.2 mm, and an unconnected length of 20 mm (a type A gusset plate).

† Finite element failure load of a specimen with an out-of-straightness of $L/1000$.

‡ Ratio of finite element failure load of a specimen with an out-of-straightness of L/1000 to finite element failure load for a shorter intermediate length specimen with the same out-of-straightness and a gusset plate width of 150 mm, thickness of 10.2 mm, and an unconnected length of 20 mm (a type A gusset plate). F_y = 300 MPa.

by Temple (1996). The simple-column approach, as explained before, assumes that the angle is a centroidally loaded column that buckles about the *z* axis, the minor principal axis of the angle. The effective length factor is usually taken as 1.0 and that assumption has been used in these calculations. The resistance factor, ϕ, was taken as 1.0. In the beam-column approach, the load was assumed to act at the centre of the gusset plate and, once again, the resistance factor was taken as 1.0.

The simple-column approach underestimates the experimental load-carrying capacity by about 30–40% for the slender specimens and by about 20–30% for the longer intermediate length specimens, but overestimates the load-carrying capacity by as much as 15% for the shorter intermediate length specimens. The fact that the simple-column approach overestimates the load-carrying capacity of shorter angles has been noted before in the literature (e.g., Woolcock and Kitipornchai 1986). This is undoubtedly due to the fact that shorter axially loaded members are more of a strength problem and, hence, the end conditions are of less importance than they are for slender angles. The beam-column approach predicts a load-carrying capacity that is only about 50%, or less, of the actual load-carrying capacity. This approach is not widely used by design engineers, since it provides a very conservative estimate of the load-carrying capacity and since it involves tedious calculations for a member that most engineers consider to be a very simple member.

The experimental results indicate the significant effect that the gusset plate has on the load-carrying capacity of the angle. Increasing the thickness of the gusset plate from 10.2 to 12.7 mm (a 24.5% increase) increased the failure load of a slender angle by 15.3%. This result is shown in column 4 of Table 2. Increasing the gusset plate width, on the other hand, from 150 to 225 mm (a 50% increase) only increases the failure load by 12.9%. A doubling of the unconnected gusset plate length did not have a significant effect on the load-carrying capacity.

For the intermediate length specimens, similar results were obtained but the percentage increases are smaller (see column 4 in Tables 3 and 4). This is to be expected as the end conditions are not as important as they are for more slender columns.

Failure modes

All the specimens failed in a similar manner. Increasing the compressive load caused some yielding to occur at the ends of the gusset plate. This was followed, in most cases, by the development of a plastic hinge at the ends of the gusset plates as the applied load increased. Such a plastic hinge can be seen in Fig. 8. Large lateral deflections of the angle at mid-height caused yielding near the toes of the angle legs which soon propagated toward the heel and then toward the ends of the angles. This yielding can be seen in Fig. 9. For slender angles, yielding of the angle was limited to the tips at mid-height only and occurred as a result of the large lateral deflections that developed after reaching the ultimate load-carrying capacity. For the shorter intermediate length specimens, yielding of the angle at mid-height started before the ultimate load was reached and kept propagating toward the ends of the angle until the failure load was reached. This behaviour was observed during the application of the load by watching the cracking of the whitewash. This failure mechanism was confirmed by the finite element analysis.

Rotation of the angle at mid-height was very small until the ultimate load was reached. At the ultimate load, the measured rotations ranged from 3.4° to 5.3° for the slender specimens, 2.8° to 4.0° for the longer intermediate length

Table 5. Experimental results and predicted compressive resistance using the two design approaches.

Specimen (1)	F_y (MPa) (2)	P_{expt} (kN) (3)	P_{sc}* (kN) (4)	$\frac{P_{expt} - P_{sc}}{P_{expt}}$ (%) (5)	P_{bc}† (kN) (6)	$\frac{P_{expt} - P_{bc}}{P_{expt}}$ (%) (7)
L-A-1	349.4	89.3	60.0	+32.8	34.0	+61.9
L-A-2	356.7	90.1	60.1	+33.3	34.2	+62.0
L-A-3	376.3	89.5	60.5	+32.4	34.7	+61.2
L-B-1	356.7	85.8	58.2	+32.2	33.3	+61.2
L-B-2	376.2	86.5	58.5	+32.4	33.8	+60.9
L-B-3	344.8	87.3	58.0	+33.6	33.0	+62.2
L-F-1	390.7	103.7	60.7	+41.5	34.3	+66.9
L-F-2	344.8	101.2	59.9	+40.8	33.0	+67.4
L-F-3	367.0	105.1	60.3	+42.6	33.7	+67.9
L-J-1	382.9	99.3	60.6	+39.0	34.9	+64.9
L-J-2	382.9	100.2	60.6	+39.5	34.9	+65.2
L-J-3	404.3	104.1	60.8	+41.6	35.4	+66.0
M-A-1	417.1	131.4	102.9	+21.7	53.4	+59.4
M-A-2	398.2	128.7	102.1	+20.7	52.6	+59.1
M-A-3	404.3	132.1	102.4	+22.5	52.8	+60.0
M-F-1	390.7	146.1	101.8	+30.3	50.8	+65.2
M-F-2	344.8	135.0	99.4	+26.4	48.3	+64.2
M-F-3	367.0	144.3	100.6	+30.3	49.6	+65.6
M-J-1	382.9	141.0	101.4	+28.1	51.8	+63.6
M-J-2	376.2	137.2	101.1	+26.3	51.5	+62.5
M-J-3	376.3	135.4	101.1	+25.3	51.5	+62.0
S-A-1	374.8	163.3	186.3	–14.1	77.5	+52.5
S-A-2	381.1	161.9	187.6	–15.9	78.4	+51.6
S-A-3	400.6	165.4	191.5	–15.8	80.9	+51.1
S-B-1	374.8	156.0	178.1	–14.2	75.6	+51.5
S-B-2	381.1	160.7	179.3	–11.6	76.5	+52.4
S-B-3	354.7	155.0	174.2	–12.4	73.0	+52.9
S-F-1	374.8	172.9	186.3	–7.8	74.6	+56.9
S-F-2	381.1	179.2	187.6	–4.7	75.4	+57.9
S-F-3	381.1	171.1	187.6	–9.6	75.4	+55.9
S-J-1	390.7	180.6	189.5	–4.9	79.7	+55.9
S-J-2	381.1	176.7	187.6	–6.2	78.4	+55.6
S-J-3	400.6	182.1	191.5	–5.2	80.9	+55.6

* Compressive resistance predicted by simple-column approach.
† Compressive resistance predicted by beam-column approach.

specimens, and 1.7° to 2.8° for the shorter intermediate length specimens.

Load–deformation curves

Figures 10 and 11 show the mid-height load–deflection and load–rotation curves for specimens L-A-1 and S-A-1, respectively. These are typical of all the curves. As can be seen, there is a good agreement between the experimental and theoretical results, but the agreement between the theoretical and experimental lateral deflections is better than that observed between the theoretical and experimental rotations. Figure 11, however, indicates that good results were obtained for even the shorter specimens. All the load versus deflection and rotation curves indicate a typical biaxial beam-column behaviour where deflections in the *x* and *y* directions and the cross-sectional rotation start increasing from the early stages of loading and increase as the load is increased. As can be observed from the load–deflection curves, the predominant deflection is the one in the *x* direction, the direction perpendicular to the gusset plate. The deflection in the plane of the gusset plate was relatively small but did increase once the ultimate load was reached. Table 6 lists the ratio of the *x* to *y* deflection for all test specimens. For the slender specimens, the lowest *x* to *y* deflection ratio observed was that of specimen L-F-2 and was 5.1 at ultimate load. At a working load, using a load factor of 1.4, the lowest *x* to *y* deflection ratio observed was for specimen L-A-3 and was 7.9. For the shorter intermediate length specimens,

Fig. 8. Plastic hinge in gusset plate.

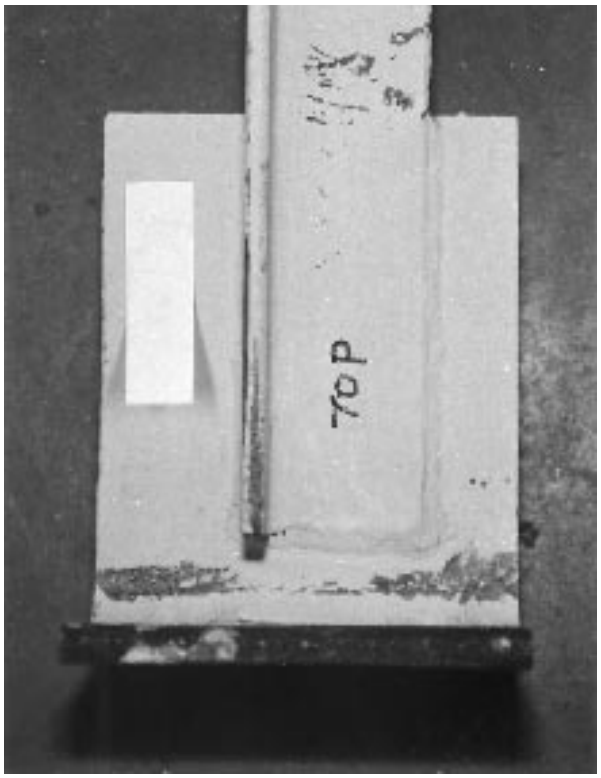

Fig. 9. Yielding of angle.

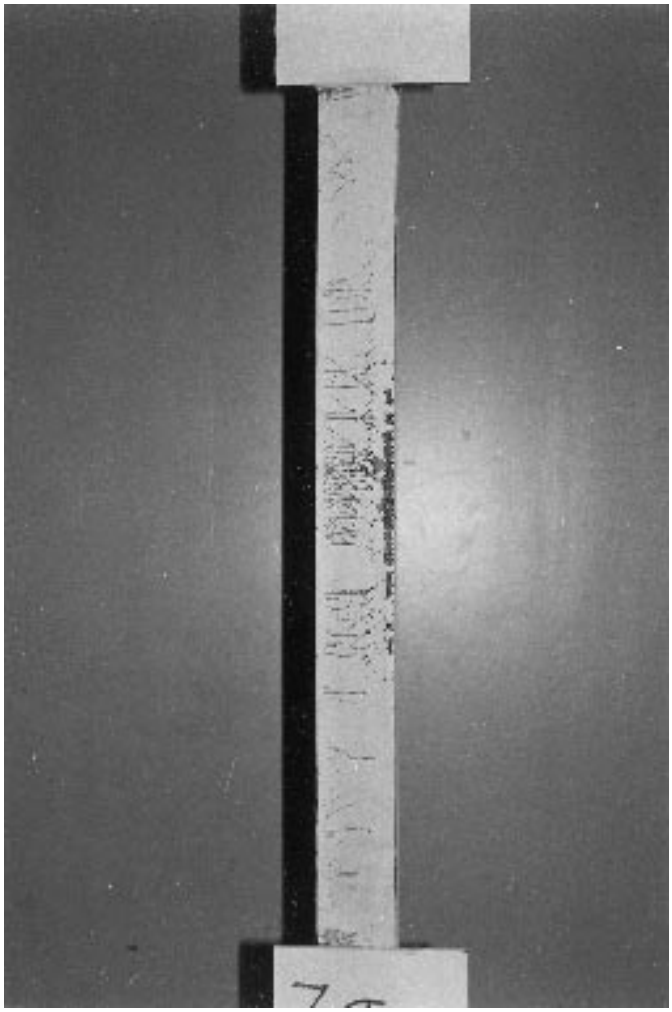

the lowest x to y deflection ratio observed was that of specimen S-J-2 and was 12.4 at ultimate load. At a working load, using, once again, a load factor of 1.4, the lowest x to y ratio observed was for specimen S-A-2 and was 12.0. This shows that all the specimens failed by flexural buckling about an axis falling between the z axis, the minor principal axis, and the y axis, the geometric axis parallel to the gusset plate. The failure axis is always very close to the y axis. The failure axis is illustrated in Fig. 12. For the slender specimens the angle α is always less than 11° at working loads and decreases to 7° or less at ultimate loads. The decrease is due to the increase in the y deflection as the ultimate load is approached. For the shorter intermediate length specimens this angle is always under 5°. The failure axis changes from one parallel to the attached leg at a section adjacent to the weld to one orientated as shown in Fig. 12 at mid-height. Table 7 shows the x to y deflection ratio for all the test specimens obtained from the finite element modelling of specimens taking the initial out-of-straightness as $L/1000$. In general, the angle is smaller than those observed in the tests.

Strain

Figure 13 shows the experimental strain measured at the end of the gusset plate of specimen L-A-3 by strain gauges 5 and 8 which are located as shown in Fig. 5. The strains at the same two points as calculated by the finite element method are also shown in the same figure. There is good agreement between the experimental and finite element results up to a load of about 75% of the ultimate load. Beyond 75% of the ultimate load, the experimental strains are much higher than those obtained using the finite element method. This might be due to residual stresses in the gusset plate which are developed as a result of the welding or manufacturing process. No attempt was made to measure these residual stresses or to account for them in the finite element analysis. It can be noted from the results that the gusset plate did not yield and develop a plastic hinge until a load was reached which is near the ultimate load for slender specimens. In the figure ε_y is the yield strain.

Figure 14 compares the experimental and finite element strains at the point where strain gauges 1 and 4 are located at mid-height of the specimen L-A-3, as indicated in Fig. 5. Comparing the finite element and experimental strains, it can be observed there is the same trend of high strain near the toe of the outstanding leg while the strain in the connected leg is almost linear. The high strain at the toe of the outstanding leg is due to the large deflections observed at mid-height near the failure load. The large deflection in the x direction is a result of the development of the plastic hinges in the gusset plates. The angle failed as a result of geometric instability caused by the large deflections at mid-height. This is to be expected, as the specimen is a slender specimen with a slenderness ratio, L/r_z, of 170.

Figure 15 shows a comparison of the experimentally measured strain and that computed by the finite element method

Fig. 10. Load versus deflection and rotation for specimen L-A-1.

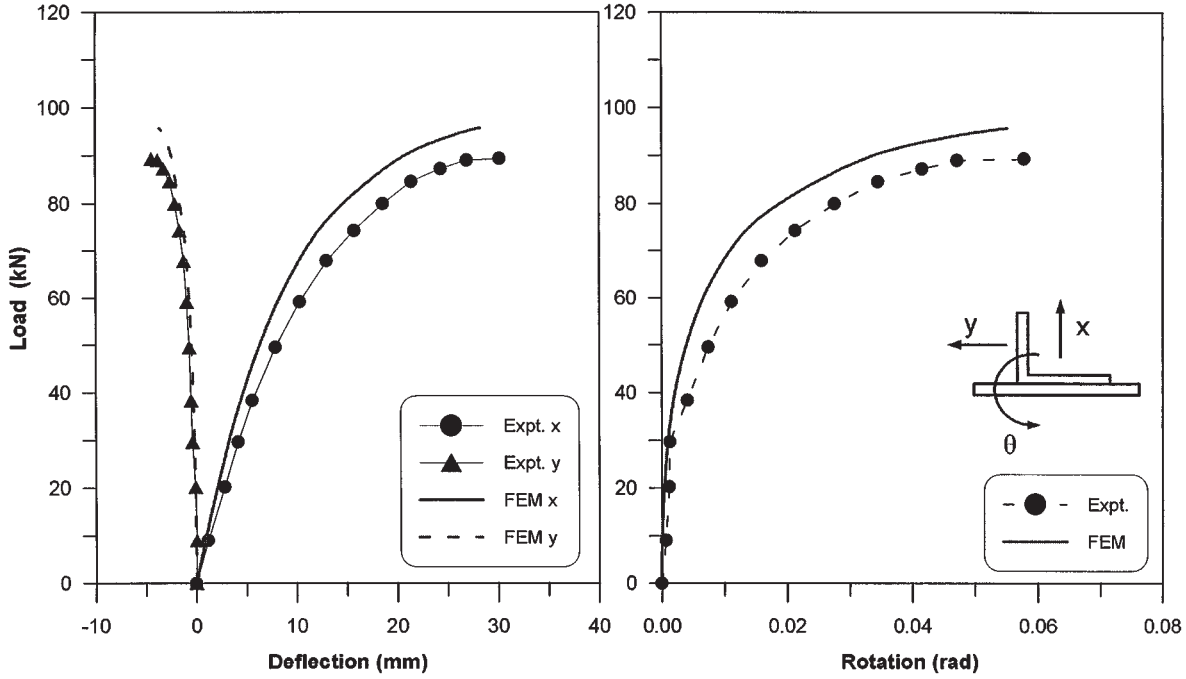

Fig. 11. Load versus deflection and rotation for specimen S-A-1.

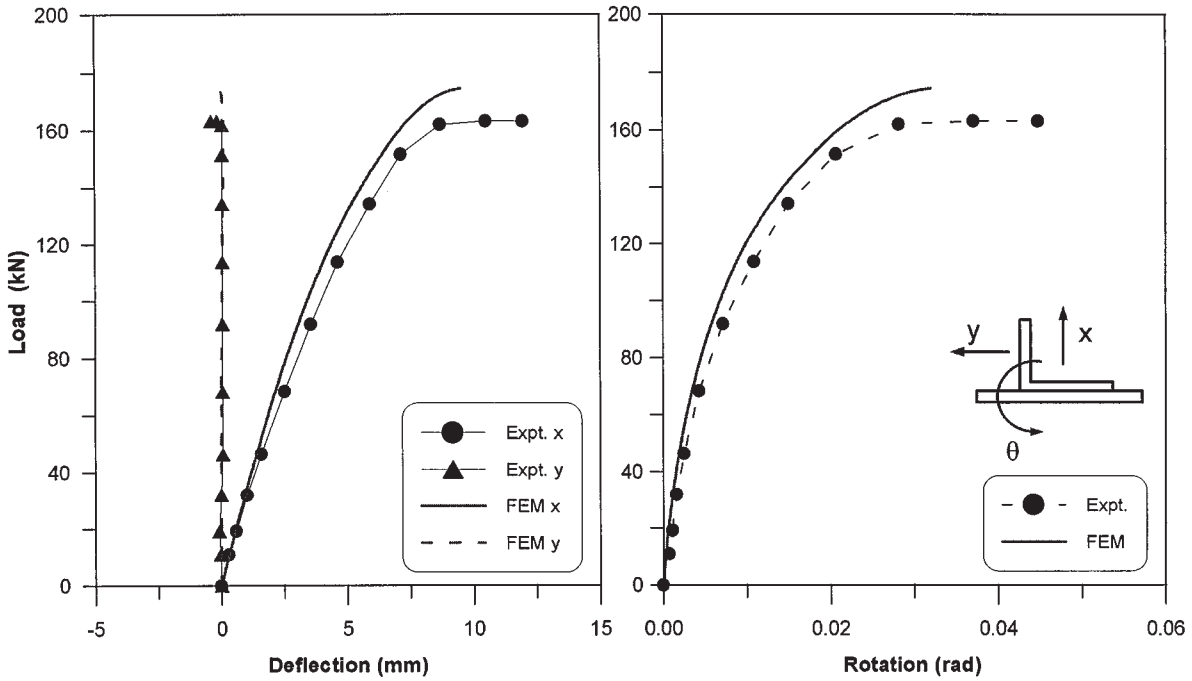

at the end of the gusset plate of the shorter intermediate length specimen S-A-3 at the location of strain gauges 5 and 8. Good agreement exists between the experimental and finite element strains until the load reaches about 95% of the ultimate load. It will be noted that the gusset plate yielded first on the compression side at a load of about 60% of the ultimate load. The plastic hinges developed in the gusset plate at a lower ratio of load to the ultimate load than with the slender specimens.

Figure 16 compares the experimental and finite element strains at the location of strain gauges 1 and 4 at mid-height of specimen S-A-3. The finite element strain is lower than the experimental strain when the load approaches the ultimate load. This is due to the large deflections observed at

Table 6. Ratio of deflections, *x*/*y*, for all test specimens.

	x/*y*			*x*/*y*			*x*/*y*	
Specimen	Working load*	Ultimate load	Specimen	Working load*	Ultimate load	Specimen	Working load*	Ultimate load
L-A-1	10.6	6.8	M-A-1	39.8	12.6	S-A-1	66.0	32.0
L-A-2	21.0	8.6	M-A-2	24.3	9.7	S-A-2	12.0	130.4
L-A-3	7.9	5.2	M-A-3	17.4	7.9	S-A-3	17.1	53.0
L-B-1	12.6	7.1				S-B-1	101.2	17.5
L-B-2	8.5	5.9				S-B-2	201.0	101.0
L-B-3	8.5	5.8				S-B-3	27.6	41.7
L-F-1	10.2	5.4	M-F-1	61.7	15	S-F-1	59.3	27.3
L-F-2	14.0	5.1	M-F-2	22.6	11.1	S-F-2	29.5	17.9
L-F-3	262.0	9.9	M-F-3	21.3	11.9	S-F-3	164.0	29.0
L-J-1	11.1	6.3	M-J-1	20.9	12.4	S-J-1	66.6	260.0
L-J-2	11	5.6	M-J-2	13	10.7	S-J-2	56.6	12.4
L-J-3	15.7	9.1	M-J-3	17.5	10.4	S-J-3	17.5	29.9

* Ratio of deflections at working load when the working load is taken as the ultimate load divided by a factor of 1.4.

mid-height near failure after the development of the plastic hinges in the gusset plates. From these curves the yielding in the attached leg can be observed at mid-height. It can be noted from the comparison that the tensile strains are higher in the finite element model while the compressive strains are lower than those measured in the laboratory. This is probably due to the initial out-of-straightness which is difficult to measure precisely in the laboratory. The curves can be shifted toward each other by changing the initial imperfection values used in the finite element model.

From Figs. 13–16 it can be concluded that a finite element analysis can be used to predict, with a reasonable degree of accuracy, the strains in the angles and in the gusset plates. This is true for all slenderness ratios studied in the experimental program. The good agreement between the experimental and finite element strains makes the finite element model a good, and economical, tool for studying the behaviour of this type of compression member. It eliminates the need for the time-consuming and costly installation of strain gauges for further studies of this type of member.

Fig. 12. Failure axis.

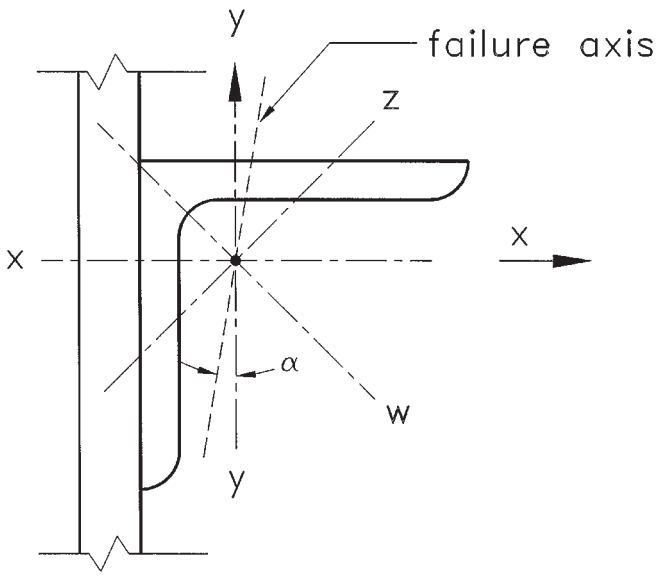

Finite element model

One of the main objectives of the experimental study was to obtain data that could be used to verify the results obtained from the finite element analysis so that the model could be used for an extensive parametric study. This parametric study was used to determine the effect of gusset plate dimensions on the behaviour and ultimate load-carrying capacity of single-angle compression members attached by one leg to a gusset plate.

In a companion paper (Temple and Sakla 1998), a parametric study is described in which the effects of changing the unconnected length, L_g, the gusset plate thickness, t_g, and the gusset plate width, B_g, are examined. It is shown that changing the unconnected length of the gusset plate has a minimal effect on the load-carrying capacity. The gusset plate thickness and width, on the other hand, have a significant effect on the load-carrying capacity.

Conclusions

In this research the behaviour and load-carrying capacity of single-angle compression members welded by one leg to a gusset plate was studied. Emphasis was placed on comparing the experimental and finite element results so that the finite element method can be used in place of a very expensive experimental study to do a parametric study of this type of member.

The following conclusions may be stated as a result of this research:

1. The finite element model used in this research can be used to predict, reasonably accurately, the behaviour and load-carrying capacity of single-angle compression members attached by one leg to a gusset plate.
2. For these angles the residual stresses can be neglected. This has been observed previously for similar members.

Table 7. Ratio of deflections, *x*/*y*, for test specimens with an initial out-of-straightness of *L*/1000 (F_y = 300 MPa).

	x/*y*			*x*/*y*			x/*y*	
Specimen	Working load*	Ultimate load	Specimen	Working load*	Ultimate load	Specimen	Working load*	Ultimate load
L-A	17.4	10.1	M-A	87	29.5	S-A	23.0	31.5
L-B	17.5	10.5				S-B	21.6	35.1
L-F	17.4	9.1	M-F	87.3	21.9	S-F	21.2	30.5
L-J	19.7	10.2	M-J	102	28.7	S-J	17.0	20.0

* Ratio of deflections at working load when the working load is taken as the ultimate load divided by a factor of 1.4.

Fig. 13. Load versus strain for specimen L-A-3, strain gauges 5 and 8.

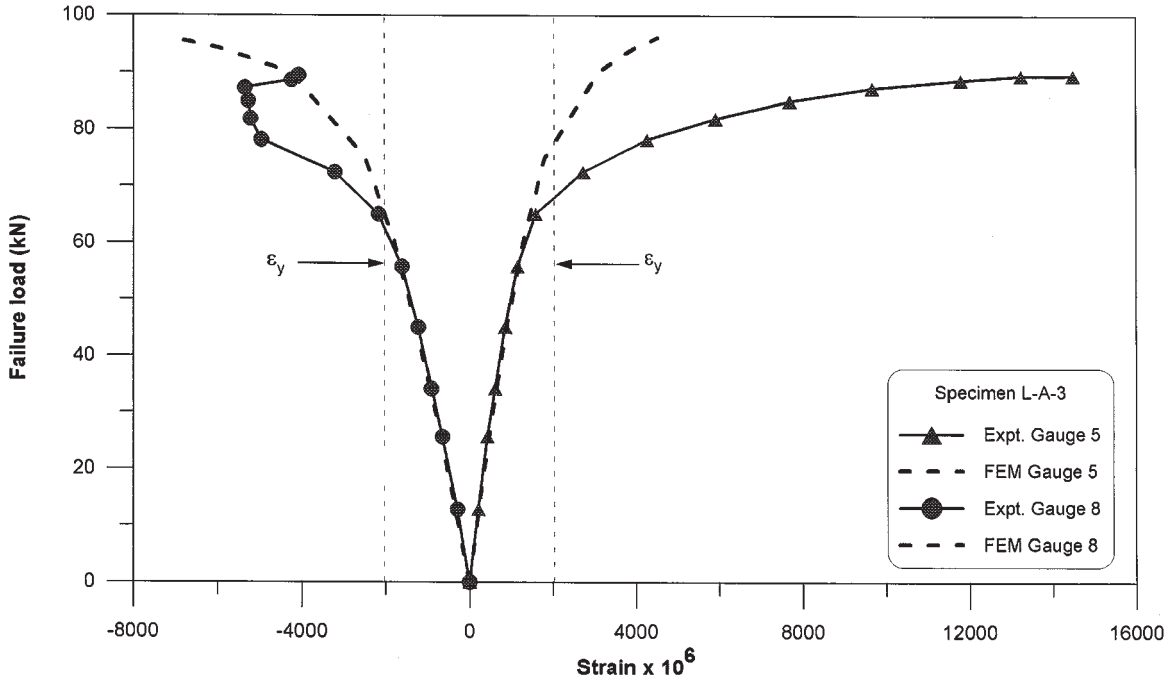

Fig. 14. Load versus strain for specimen L-A-3, strain gauges 1 and 4.

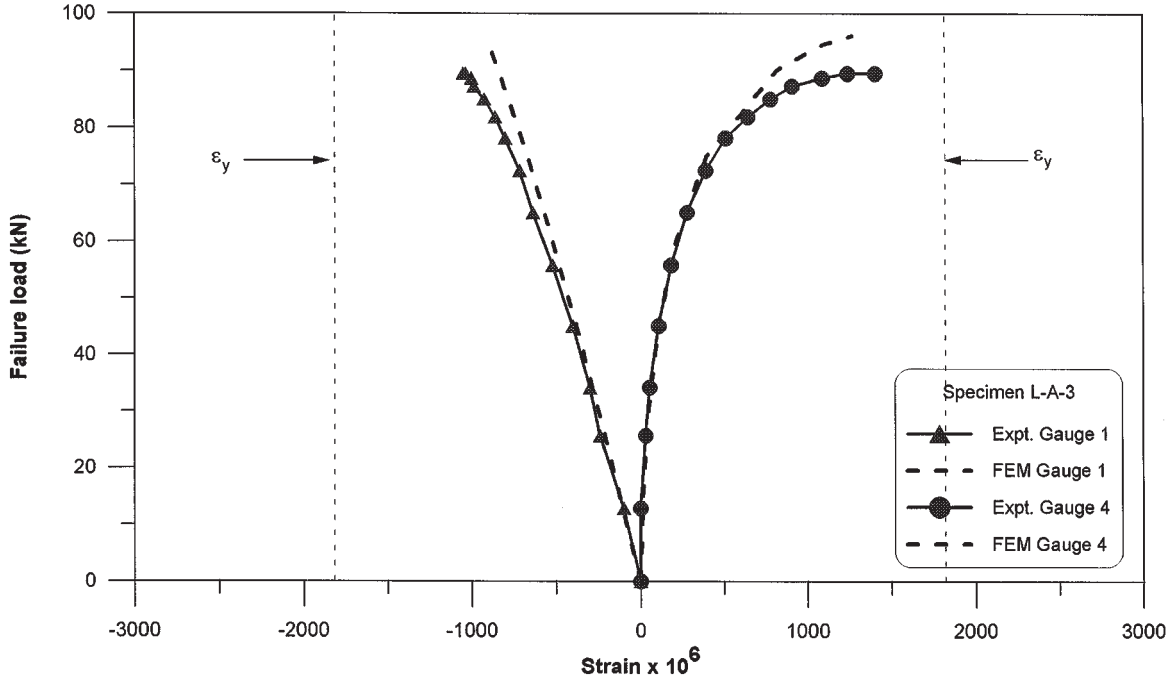

Fig. 15. Load versus strain for specimen S-A-3, strain gauges 5 and 8.

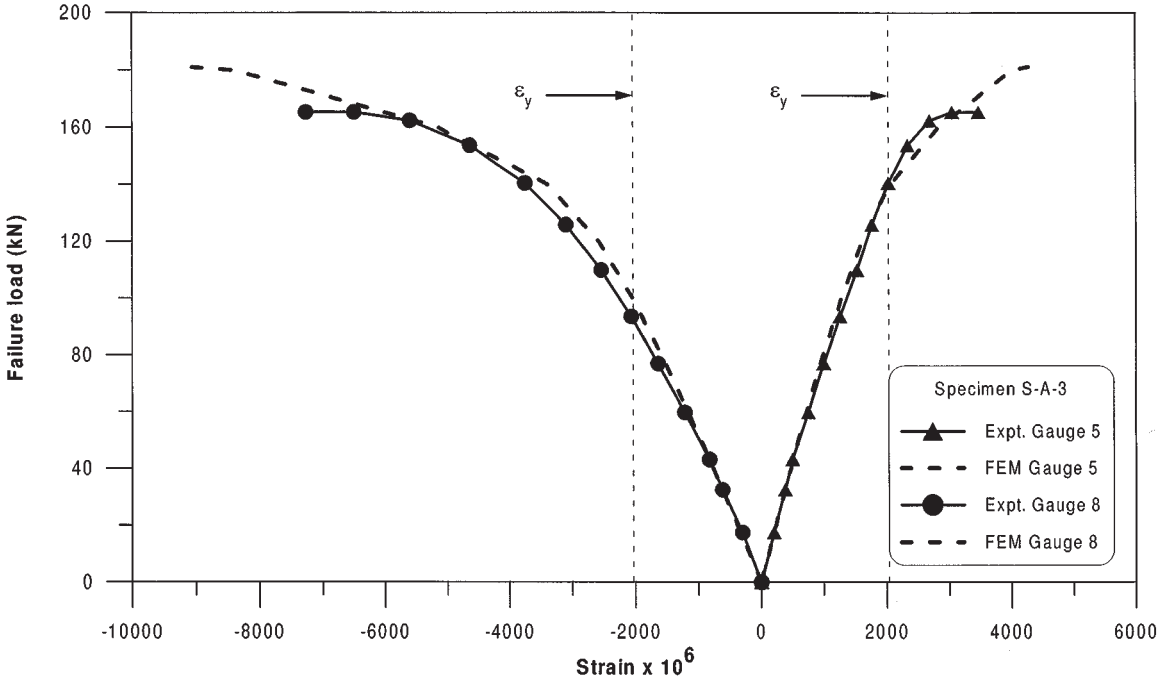

Fig. 16. Load versus strain for specimen S-A-3, strain gauges 1 and 4.

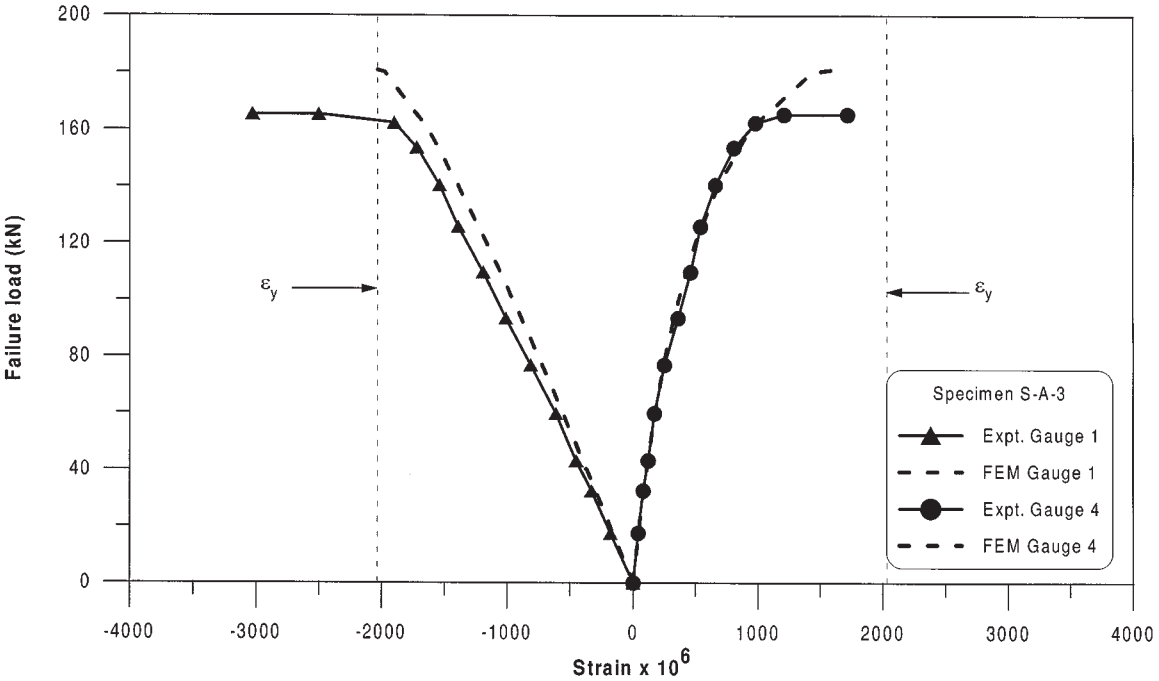

The residual stresses at the location of the plastic hinge did not have a great effect on the experimental load-carrying capacity, since the finite element results were in good agreement with the experimental results.

3. The failure was initiated by yielding of the gusset plate. In most cases this was followed by the development of a plastic hinge. The angle failed, primarily, because of excessive deflection in a direction perpendicular to the gusset plate.
4. The dimensions of the gusset plate have a significant effect on the behaviour and load-carrying capacity and should be accounted for in the design procedure.
5. The beam-column approach greatly underestimates the load-carrying capacity of these members. The simple-

column approach also underestimates the load capacity except for members with small slenderness ratios.

Acknowledgments

The continued support of the Natural Sciences and Engineering Research Council of Canada is gratefully acknowledged.

References

AISC. 1994. Manual of steel construction, load and resistance factor design. American Institute of Steel Construction, Chicago, Ill.

CISC. 1995. Handbook of steel construction. Canadian Institute of Steel Construction, Willowdale, Ont.

CSA. 1989. Limit states design of steel structures. Standard CAN/CSA-S16.1-M89, Canadian Standards Association, Rexdale, Ont.

CSA. 1992. General requirements for rolled or welded structural quality steel. Standard CAN/CSA-G40.20-M92, Canadian Standards Association, Rexdale, Ont.

ECCS. 1985. Recommendations for angles in lattice transmission towers. Working Group 8.1, Technical Committee 8, European Convention for Constructional Steel Work, Brussels, Belgium.

Elgaaly, M., Davids, W., and Dagher, H. 1992. Non-slender single angle struts. Engineering Journal, American Institute of Steel Construction, **29**(2): 49–58.

Girard, C., Picard, A., and Farad, M. 1995. Finite element modelling of shear lag effects in an HSS welded to a gusset plate. Canadian Journal of Civil Engineering, **22**(4): 651–659.

Hibbitt, Karlson and Sorenson, Inc. 1994. ABAQUS, version 5.4. Hibbitt, Karlson and Sorenson, Inc., Providence, R.I.

Johnston, B.G. (*Editor*). 1966. The guide to design criteria for metal compression members. 2nd ed. John Wiley & Sons, New York.

Leigh, J.M., and Galambos, T.V. 1972. The design of compression webs in long span steel joists. Structural Division, Department of Civil and Environmental Engineering, Washington University, St. Louis, Mo., Research Report, No. 21.

Lipson, S.L., and Haque, M.I. 1978. Elastic-plastic analysis of single-angle bolted-welded connection using the finite element method. Computers and structures, **9**: 533–545.

Temple, M.C. 1996. Design of single-angle compression members according to the Canadian standards. Canadian Journal of Civil Engineering, **23**(3): 632–638.

Temple, M.C., and Sakla, S.S.S. 1996. Considerations for the design of single-angle compression members attached by one leg. Canadian Journal of Civil Engineering, **23**(1): 287–294

Temple, M C., and Sakla, S.S.S. 1998. Single-angle compression members welded by one leg to a gusset plate. II. A parametric study and design equation. Canadian Journal of Civil Engineering, **25**: 585–594.

Trahair, N.S., Usami, T., and Galambos, T.V. 1969. Eccentrically loaded single-angle columns. Structural Division, Department of Civil and Environmental Engineering, Sever Institute of Technology, St. Louis, Mo., Research Report No. 11.

Usami, T., and Galambos, T.V. 1971. Eccentrically loaded single-angle columns. Proceedings of the International Association for Bridge and Structural Engineering Conference, Zurich, Switzerland, pp. 153–183.

Woolcock, S.T., and Kitipornchai, S. 1980. The design of single angle struts. Steel Construction, Australian Institute of Steel Construction, **14**(4): 2–23.

Woolcock, S.T., and Kitipornchai, S. 1986. Design of single-angle web struts in trusses. ASCE Journal of Structural Engineering, **112**(6): 1327–1345.

List of symbols

A: cross-sectional area of angle
B_g: width of gusset plate
C_m: equivalent moment factor for beam-columns
E: Young's modulus of elasticity
F_a: applied compressive stress due to axial load and bending
F_{CRC}: Column Research Council basic column strength formula
F_y: yield stress
I_y: moment of inertia about the y axis
K: effective length factor
L: length of the angle
L_g: unconnected length of gusset plate
L_w: weld length on each side of angle leg
M_y: moment about the y axis required to produce compressive yielding in the extreme fibre when axial load is zero
M_1, M_2: bending moments acting at the ends of the member taking into account the end restraint caused by the truss chords; M_1 is numerically greater than M_2
P: axial compressive load
P_E: Euler load about the y axis
P_o: axial load-carrying capacity in the absence of bending
r_y: radius of gyration about the y axis, a geometric axis
r_z: radius of gyration about the z axis, the minor principal axis
t_g: thickness of gusset plate
y: distance from the angle centroid to its compressive edge
ε_y: yield strain
ϕ: resistance factor